

Solvation dynamics in coherent and spontaneous Raman spectroscopy: application to β -carotene

James Sue and Shaul Mukamel

Department of Chemistry, University of Rochester, Rochester, New York 14627

Received December 8, 1987; accepted February 29, 1988

A stochastic theory of the nonlinear susceptibility $\chi^{(3)}$ is used to analyze coherent and spontaneous Raman spectra of polyatomic molecules in solution. The theory holds for any solvation time scale and interpolates between the homogeneous limit, in which the Bloch equations are valid, and the static limit of inhomogeneous line broadening, as the solvent time scale is increased. Application is made to β -carotene in alkanes and in CS_2 . The calculated spontaneous Raman profiles are found to be in good agreement with experiment, and the coherent Raman excitation profiles are predicted. The magnitude of the solvent-solute interaction and the solvation time scale for various solvents are obtained from our theoretical analysis. The relative contribution of inhomogeneous line broadening in isopentane is found to increase as the temperature is raised from 118 to 298 K.

1. INTRODUCTION

Coherent Raman spectroscopy is a four-wave mixing technique that provides a sensitive spectroscopic probe for dynamic processes of polyatomic molecules in condensed phases. Coherent Raman measurements usually involve two applied fields with wave vectors \mathbf{k}_L and \mathbf{k}_L' (Fig. 1) and detection of the signal mode with wave vector \mathbf{k}_S and frequency ω_S , where¹⁻⁴

$$\mathbf{k}_S = 2\mathbf{k}_L - \mathbf{k}_L', \quad (1a)$$

$$\omega_S = 2\omega_L - \omega_L'. \quad (1b)$$

If the frequency of one laser is fixed and the other laser is scanned, the coherent Raman spectra show narrow resonances (width $\lesssim 10 \text{ cm}^{-1}$) superimposed upon a broad background (width $\sim 100 \text{ cm}^{-1}$). This is similar to what is observed in ordinary spontaneous Raman spectroscopy, in which sharp Raman lines and a broad fluorescence are usually observed.⁴⁻⁹ However, resonances in spontaneous Raman spectroscopy occur only between vibrational states of the ground electronic state, whereas in coherent Raman spectroscopy resonances may also occur between vibrational states of the excited electronic state.^{3,10} In this paper we analyze and compare coherent and spontaneous Raman line shapes of polyatomic molecules in condensed phases (e.g., solution, solid matrices, and glasses) by using a stochastic theory of the nonlinear susceptibility $\chi^{(3)}$.³⁻⁵ In Section 2 we briefly present our model and analyze the coherent anti-Stokes Raman spectroscopy (CARS) line shapes in several limits of physical interest. Expressions are derived for the nonlinear susceptibility $\chi^{(3)}$ and for the CARS excitation profiles that are the coherent analog of spontaneous Raman excitation profiles. Coherent experiments offer many worthwhile advantages, such as good signal discrimination and fluorescence rejection through spatial and spectral filtering, and this technique is expected to gain further attention in the future with the development of tunable lasers. In Section 3 we make an application to β -carotene in isopen-

tane, in 1:1 pentane-isopentane, and in CS_2 and calculate the absorption line shape and spontaneous Raman excitation profiles. The calculations are compared with experiments, with good agreement, and solvent parameters (the magnitude of the solvent-solute interaction and its correlation time) are obtained. We then predict the CARS excitation profiles for the same systems. In Section 4 we summarize our results.

2. COHERENT ANTI-STOKES RAMAN SPECTROSCOPY EXCITATION SPECTRA

We consider a nonlinear medium consisting of molecules with two electronic states interacting with a classical electromagnetic field. We assume a model consisting of a system with a few relevant optically active vibrational modes and a bath comprising the remaining weakly active modes of the molecule and the solvent. Hereafter we use the term solvent to include also the weakly active modes and use the words solvent and bath interchangeably. We also refer to the system as the molecule. We assume that the random force exerted on the molecules by their environment makes the electronic energy gap ω_{eg} a stochastic function of time (Fig. 2). The total Hamiltonian assumes the form^{3-5,7,8}

$$H_T = H + H_{\text{int}}. \quad (2)$$

Here H_{int} represents the radiation-matter interaction, and H is the Hamiltonian for the material system in the absence of the radiation field and is given by

$$H = |g\rangle H_g \langle g| + |e\rangle [\omega_{eg} + \delta\omega_{eg}(t) + H_e] \langle e|, \quad (3)$$

where $H_g(H_e)$ is the nuclear Hamiltonian corresponding to the electronic state $|g\rangle(|e\rangle)$, ω_{eg} is the mean electronic energy gap (0-0 transition), and $\delta\omega_{eg}(t)$ is assumed to be a stochastic Gaussian-Markov process with zero mean,

$$\langle \delta\omega_{eg}(t) \rangle = 0, \quad (4a)$$

and its correlation function is

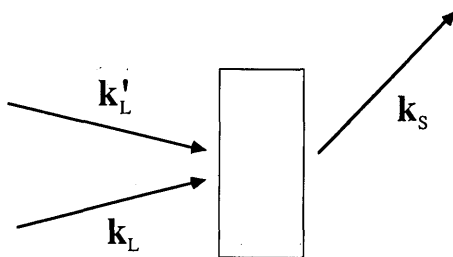


Fig. 1. CARS four-wave mixing process. The two incident laser fields \mathbf{k}_L and \mathbf{k}_L' interact nonlinearly with the medium and generate the signal field \mathbf{k}_S .

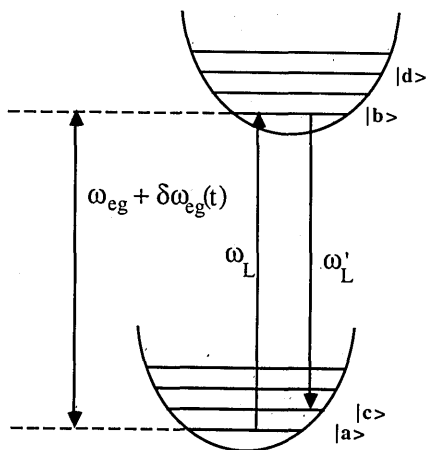


Fig. 2. Molecular-level scheme and laser frequencies for CARS. Levels $|a\rangle$ and $|c\rangle$ are part of the ground-state vibrational manifold, whereas levels $|b\rangle$ and $|d\rangle$ belong to an electronically excited manifold. The electronic-dipole operator couples vibronic states belonging to different electronic states.

$$\langle \delta\omega_{eg}(t)\delta\omega_{eg}(0) \rangle = \Delta^2 \exp(-\Lambda t). \quad (4b)$$

The angle brackets denote averaging over the stochastic variables. Δ is the amplitude of the stochastic modulation, and Λ^{-1} is its time scale (correlation time). The states $|a\rangle$, $|c\rangle$, etc. (Fig. 2) are the vibrational eigenstates of H_g ,

$$H_g|j\rangle = (\epsilon_j - i\gamma_j)|j\rangle, \quad j = a, c, \dots, \quad (5a)$$

whereas the states $|b\rangle$, $|d\rangle$ are the vibronic eigenstates of H_e , i.e.,

$$(\omega_{eg} + H_e)|j\rangle = (\epsilon_j - i\gamma_j)|j\rangle, \quad j = b, d, \dots \quad (5b)$$

Here ϵ_j and γ_j are the energy and the inverse lifetime, respectively, of state $|j\rangle$.

In coherent Raman spectroscopy we look for narrow two-photon resonances in the signal, which occur when $\omega_L - \omega_L'$ equals an energy difference between two vibrational states belonging either to the ground electronic state or to an excited electronic state. For our level scheme (Fig. 2) such resonances occur for $\omega_L - \omega_L' = \pm\omega_{ca}$ and for $\omega_L - \omega_L' = \pm\omega_{db}$. CARS and coherent Stokes Raman spectroscopy refer to the cases in which $\omega_L > \omega_L'$ and $\omega_L < \omega_L'$, respectively. Since there are no fundamental differences between the theoretical treatments of the two, we shall focus on the CARS resonances located at

$$\omega_L - \omega_L' = \omega_{ca}, \quad (6a)$$

$$\omega_L - \omega_L' = \omega_{db}, \quad (6b)$$

where

$$\omega_{\mu\nu} \equiv \epsilon_\mu - \epsilon_\nu, \quad \mu, \nu = a, b, c, d. \quad (6c)$$

Equation (6a) represents a ground-state CARS resonance and Eq. (6b) represents an excited-state CARS resonance. The general expression for the nonlinear susceptibility $\chi^{(3)}$ that describes any four-wave mixing experiment (and in particular CARS) for this model has been given.³⁻⁵ The CARS signal S_{CARS} generated at $\mathbf{k}_S = 2\mathbf{k}_L - \mathbf{k}_L'$ is defined as the rate of photon emission into mode S and is

$$S_{\text{CARS}}(\mathbf{k}_S) = |\chi_{\text{CARS}}^{(3)}(-\omega_S; \omega_L, -\omega_L', \omega_L)|^2. \quad (7)$$

The third-order nonlinear susceptibility for the CARS process within the rotating-wave approximation is given by

$$\chi_{\text{CARS}}^{(3)}(-\omega_S; \omega_L, \omega_L', \omega_L) = \sum_{a,c} \chi_{ca}^{(3)} + \sum_{b,d} \chi_{bd}^{(3)}, \quad (8)$$

where

$$\begin{aligned} \chi_{ca}^{(3)} = & \sum_{n=0}^{\infty} \frac{1}{n!k^{2n}} \sum_{b,d} \mu_{ab} \mu_{bc} \mu_{cd} \mu_{da} \\ & \times \frac{J_n(2\omega_L - \omega_L' - \omega_{ba} + i\gamma_{ba})}{\omega_L - \omega_L' - \omega_{ca} + i(\gamma_{ca} + n\Lambda)} \\ & \times [P(a)J_n(\omega_L - \omega_{da} + i\gamma_{da}) \\ & + (-1)^n P(c)J_n(\omega_{dc} - \omega_L' + i\gamma_{dc})], \end{aligned} \quad (9a)$$

$$\begin{aligned} \chi_{db}^{(3)} = & \sum_{n=0}^{\infty} \frac{1}{n!k^{2n}} \sum_{a,c} P(a) \mu_{ab} \mu_{bc} \mu_{cd} \mu_{da} \\ & \times \frac{J_n(2\omega_L - \omega_L' - \omega_{dc} + i\gamma_{dc})}{\omega_L - \omega_L' - \omega_{db} + i(\gamma_{db} + n\Lambda)} \\ & \times [J_n(\omega_L - \omega_{da} + i\gamma_{da}) \\ & + (-1)^n J_n(\omega_{ba} - \omega_L' + i\gamma_{ba})], \end{aligned} \quad (9b)$$

with

$$J_n(s) = -i \int_0^{\infty} d\tau [1 - \exp(-\Lambda\tau)]^n \exp[is\tau - g(\tau)], \quad n = 0, 1, 2, \dots, \quad (10a)$$

$$g(\tau) = \frac{\Delta^2}{\Lambda^2} [\exp(-\Lambda\tau) - 1 + \Lambda\tau], \quad (10b)$$

$$\kappa \equiv \Lambda/\Delta, \quad (10c)$$

and

$$\gamma_{\mu\nu} = \gamma_\mu/2 + \gamma_\nu/2. \quad (10d)$$

$\chi_{ac}^{(3)}$ is the part of the nonlinear susceptibility that contributes to the ground-state CARS resonances at $\omega_L - \omega_L' = \omega_{ca}$, and $\chi_{db}^{(3)}$ is the part that contributes to the excited-state CARS resonances at $\omega_L - \omega_L' = \omega_{db}$. The two pathways in Liouville space that contribute to $\chi_{ac}^{(3)}$ are shown in Figs. 3(a) and 3(b). The two pathways that contribute to $\chi_{db}^{(3)}$

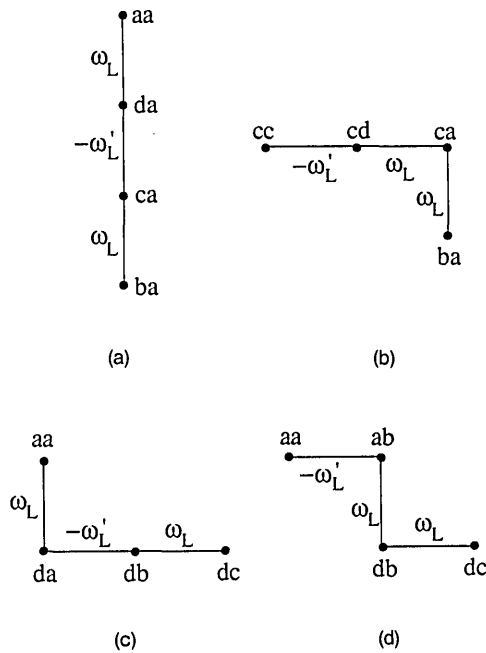


Fig. 3. Pictorial representation of the four Liouville pathways^{3,5} that contribute to CARS within the rotating-wave approximation. Each line represents a radiative interaction with a laser field with the indicated frequency.

are shown in Figs. 3(c) and 3(d). These diagrams show the order in time of the radiative interactions with the radiation fields ω_L and ω_L' and whether these interactions are with the bra or with the ket of the density matrix. Each diagram starts with the aa or cc state in the upper left-hand corner. A radiative interaction acting from the left (bra) is represented by a vertical line, whereas an interaction from the right (ket) is represented by a horizontal line. Each diagram has three interactions. Each interaction line is labeled by the proper field (ω_L or ω_L'). For a more-detailed discussion of the diagrams see Ref. 3. $P(a)$ is the equilibrium population of state $|a\rangle$, and $J_n(s)$ are stochastic line-shape functions that may be efficiently calculated by using continued fractions.^{4,7,8} The nature of the broadening depends primarily on the parameter $\kappa \equiv \Lambda/\Delta$. As κ increases, the broadening varies from homogeneous to inhomogeneous.^{3-5,7-9} In the homogeneous limit ($\kappa \rightarrow \infty$) we can eliminate the summation over n in Eqs. (9a) and (9b) and retain only the $n = 0$ terms. $g(\tau)$ then assumes the form $g(\tau) = (\Delta^2/\Lambda)\tau$. In this case, Eqs. (8)–(10) reduce to the conventional results of $\chi^{(3)}$ derived by using the Bloch equations^{1,2} with a dephasing rate of Δ^2/Λ . It may be more convenient to parameterize our broadening model in terms of the full width at half-maximum Γ_0 and κ rather than Δ and Λ . Γ_0 is given approximately by^{7,8}

$$\Gamma_0/\Delta = \frac{2.355 + 1.76\kappa}{1 + 0.85\kappa + 0.88\kappa^2}. \quad (11)$$

In a typical CARS experiment the two observables of interest are the coherent Raman spectra and the CARS excitation profiles. A Raman spectrum is obtained by fixing ω_L and tuning ω_L' . The resulting spectrum consists of sharp lines at the molecular Raman excitation frequencies, superimposed upon a much broader background. CARS excitation profiles, on the other hand, are obtained by measuring

the intensity of a particular Raman line while tuning both ω_L and ω_L' and keeping $\omega_L - \omega_L'$ fixed ($\omega_L - \omega_L' = \omega_{ca}$ for a ground-state CARS excitation profile and $\omega_L - \omega_L' = \omega_{db}$ for an excited-state CARS excitation profile). A close examination of Eqs. (9a) and (9b) shows that the terms contributing to the ν_μ Raman line consist of a series of progressively broader line shapes of widths $\gamma_{\mu\nu} + n\Lambda$, $n = 0, 1, 2, \dots$, and centered at $\omega_L - \omega_L' = \omega_{\mu\nu}$. Our procedure to define the Raman excitation profiles is as follows. We introduce a cutoff $n = n^*$ such that for $n \leq n^*$, $\gamma_{\mu\nu} + n\Lambda$ is much smaller than a characteristic line broadening in solution, typically a few hundred inverse centimeters. For $n \leq n^*$, we make the approximations

$$\left| \frac{1}{\omega_L - \omega_L' - \omega_{ca} + i(\gamma_{ca} + n\Lambda)} \right|^2 \approx \frac{\pi}{\gamma_{ca} + n\Lambda} \delta(\omega_L - \omega_L' - \omega_{ca}) \quad (12a)$$

and

$$\left| \frac{1}{\omega_L - \omega_L' - \omega_{db} + i(\gamma_{db} + n\Lambda)} \right|^2 \approx \frac{\pi}{\gamma_{db} + n\Lambda} \delta(\omega_L - \omega_L' - \omega_{db}). \quad (12b)$$

These terms will thus contribute to the sharp Raman resonances. The remaining terms with $n > n^*$ contribute to the background and not to the sharp Raman lines. This separation of terms is similar to that made in our earlier treatment of spontaneous Raman and fluorescence.^{7,8} Accordingly, we shall rearrange the CARS signal Eq. (7) by using relations (12) as follows:

$$S_{\text{CARS}}(\omega_L, \omega_L') = \sum_{a,c} Q_{ac}^g(\omega_L) \delta(\omega_L - \omega_L' - \omega_{ca}) + \sum_{b,d} Q_{db}^e(\omega_L) \delta(\omega_L - \omega_L' - \omega_{db}) + \text{background terms}, \quad (13)$$

where

$$Q_{ca}^g(\omega_L) = |K_{ca}^g(\omega_L)|^2, \quad (14a)$$

$$Q_{db}^e(\omega_L) = |K_{db}^e(\omega_L)|^2, \quad (14b)$$

$$K_{ca}^g = \sum_{n=0}^{n^*} \frac{1}{n! \kappa^{2n}} \left(\frac{\pi}{\gamma_{ca} + n\Lambda} \right)^{1/2} \sum_{b,d} \mu_{ab} \mu_{bc} \mu_{cd} \mu_{da} \times J_n(\omega_L - \omega_{bc} + i\gamma_{ba}) [P(a) J_n(\omega_L - \omega_{da} + i\gamma_{da}) + (-1)^n P(c) J_n(\omega_{da} - \omega_L + i\gamma_{dc})], \quad (14c)$$

$$K_{db}^e = \sum_{n=0}^{n^*} \frac{1}{n! \kappa^{2n}} \left(\frac{\pi}{\gamma_{db} + n\Lambda} \right)^{1/2} \sum_{a,c} P(a) \mu_{ab} \mu_{bc} \mu_{cd} \mu_{da} \times J_n(\omega_L - \omega_{bc} + i\gamma_{dc}) [J_n(\omega_L - \omega_{da} + i\gamma_{da}) + (-1)^n J_n(\omega_{da} - \omega_L + i\gamma_{ba})]. \quad (14d)$$

Here $Q_{ac}^g(Q_{db}^e)$ is the CARS ground- (excited-) state excitation profile for the $ca(db)$ Raman line and $K_{ac}^g(K_{db}^e)$ is its amplitude. Equation (13) is based on the assumption that

the ground-state and excited-state Raman transitions are well resolved. When several Raman transitions have the same frequency $\omega_{\mu\nu} = \zeta$ (as in the case for harmonic molecules), the amplitudes for all the transitions that contribute to the resonance at $\omega_L - \omega_{L'} = \zeta$ should be summed before taking the square. The Raman excitation profile is then given instead by

$$Q^{\zeta}(\omega_L) = \left| \sum'_{a,c} K_{ca}^g(\omega_L) + \sum'_{b,d} K_{db}^e(\omega_L) \right|^2. \quad (14e)$$

The prime on the summation sign in Eq. (14e) denotes a restricted sum over the degenerate transitions.

We now analyze the CARS excitation profiles in various limits of physical interest. For simplicity, we hereafter assume that all the lifetimes of the vibrational states belonging to the same electronic state are identical, i.e., $\gamma_b = \gamma_d \equiv \gamma$ and $\gamma_a = \gamma_c \equiv \gamma'$. The analysis and the limiting cases presented here are analogous to our earlier work on spontaneous Raman line shapes.^{7,8}

A. Rapid Fluctuation Limit

The rapid fluctuation limit holds when $\gamma, \gamma' \ll \Lambda$.⁷ In this case the $n > 0$ terms in Eqs. (9) will be much broader and negligible compared with the $n = 0$ terms. Retaining only the terms with $n = 0$, we have for the Raman susceptibilities by using Eqs. (9) and relations (12)

$$\chi_{ca}^{(3)} = \sum_{b,d} \mu_{ab}\mu_{bc}\mu_{cd}\mu_{da} \frac{J_0(2\omega_L - \omega_{L'} - \omega_{ba} + i\bar{\gamma})}{\omega_L - \omega_{L'} - \omega_{ca} + i\gamma'} \times [P(a)J_0(\omega_L - \omega_{da} + i\bar{\gamma}) + P(c)J_0(\omega_{dc} - \omega_{L'} + i\bar{\gamma})] \quad (15a)$$

and

$$\chi_{db}^{(3)} = \sum_{a,b} P(a)\mu_{ab}\mu_{bc}\mu_{cd}\mu_{da} \frac{J_0(2\omega_L - \omega_{L'} - \omega_{dc} + i\bar{\gamma})}{\omega_L - \omega_{L'} - \omega_{db} + i\gamma} \times [J_0(\omega_L - \omega_{da} + i\bar{\gamma}) + J_0(\omega_{ba} - \omega_{L'} + i\bar{\gamma})], \quad (15b)$$

where

$$\bar{\gamma} = \frac{\gamma + \gamma'}{2}. \quad (16)$$

The corresponding excitation amplitudes may then be obtained by using Eqs. (14) with $n^* = 0$, resulting in

$$K_{ca}^g = \left(\frac{\pi}{\gamma'}\right)^{1/2} \sum_{b,d} \mu_{ab}\mu_{bc}\mu_{cd}\mu_{da} J_0(\omega_L - \omega_{bc} + i\bar{\gamma}) \times [P(a)J_0(\omega_L - \omega_{da} + i\bar{\gamma}) + P(c)J_0(\omega_{da} - \omega_L + i\bar{\gamma})] \quad (17a)$$

and

$$K_{db}^e = 2i \left(\frac{\pi}{\gamma}\right)^{1/2} \sum_{a,c} \mu_{ab}\mu_{bc}\mu_{cd}\mu_{da} P(a) J_0(\omega_L - \omega_{bc} + i\bar{\gamma}) \times \text{Im} J_0(\omega_L - \omega_{da} + i\bar{\gamma}). \quad (17b)$$

The rapid fluctuation limit usually holds for polyatomic molecules in solution.^{7,8}

B. Homogeneous Limit

In the homogeneous limit the inverse time scale Λ of the fluctuations of the electronic energy gap is much larger than their magnitude ($\Delta \ll \Lambda$), and we have [Eq. (10b)]^{7,8}

$$g(\tau) = (\Delta^2/\Lambda)\tau. \quad (18)$$

Substitution of Eq. (18) into Eqs. (9) and (10) results in

$$\chi_{ca}^{(3)} = \sum_{b,d} \mu_{ab}\mu_{bc}\mu_{cd}\mu_{da} \frac{1}{2\omega_L - \omega_{L'} - \omega_{ba} + i\Gamma} \times \frac{1}{\omega_L - \omega_{L'} - \omega_{ca} + i\gamma'} \times \left[\frac{P(a)}{\omega_L - \omega_{da} + i\Gamma} + \frac{P(c)}{\omega_{dc} - \omega_{L'} + i\Gamma} \right] \quad (19a)$$

and

$$\chi_{db}^{(3)} = \sum_{a,c} \mu_{ab}\mu_{bc}\mu_{cd}\mu_{da} P(a) \frac{1}{2\omega_L - \omega_{L'} - \omega_{dc} + i\Gamma} \times \frac{1}{\omega_L - \omega_{da} + i\Gamma} \frac{1}{\omega_{ba} - \omega_{L'} + i\Gamma} \times \left[1 + \frac{\hat{\Gamma} + \gamma'}{\omega_L - \omega_{L'} - \omega_{db} + i\gamma} \right], \quad (19b)$$

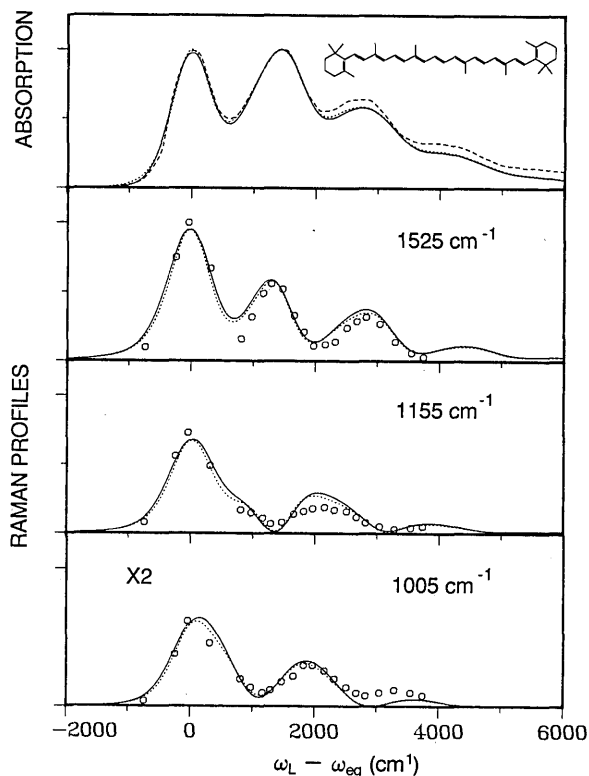


Fig. 4. Absorption $\sigma(\omega_L)$ [Eq. (32)] (upper panel) and resonance Raman profiles $Q_{ca}(\omega_L)$ [Eq. (33)] of the indicated transitions (three lower panels) of β -carotene in isopentane at 118 K. The Raman frequency is indicated in each panel. The dashed curve in the upper panel and the circles in the three lower panels are the experimental data of Ref. 14. The theoretical curves were calculated by using the structural parameters of Table 2. $\omega_{eg} = 20\,180\text{ cm}^{-1}$, and the solvent parameters are (in cm^{-1}) solid lines: $\alpha = 0$, $\Gamma_0 = 760$, $\Delta = 362$, and $\Lambda = 108$; dotted lines: $\alpha = 75$, $\Gamma_0 = 700$, $\Delta = 413$, $\Lambda = 330$.

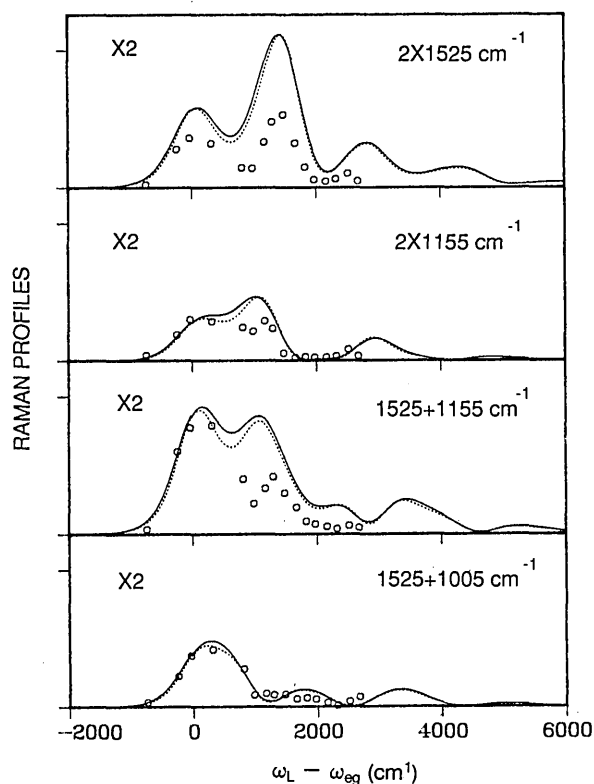


Fig. 5. Relative Raman excitation profiles of overtones and combinations of β -carotene in isopentane at 118 K. The parameters of the theoretical curves (solid and dotted lines) are as in Fig. 4. The experimental data are from Ref. 14.

where

$$\Gamma = \hat{\Gamma} + \bar{\gamma} \quad (20)$$

and

$$\hat{\Gamma} = \Delta^2/\Lambda \quad (21)$$

is the pure dephasing rate. The CARS excitation amplitudes are then given by

$$K_{ca}^g(\omega_L) = \left(\frac{\pi}{\gamma'}\right)^{1/2} \sum_{b,d} \mu_{ab}\mu_{bc}\mu_{cd}\mu_{da} \frac{1}{\omega_L - \omega_{bc} + i\Gamma} \times \left[\frac{P(a)}{\omega_L - \omega_{da} + i\Gamma} + \frac{P(c)}{\omega_{da} - \omega_L + i\Gamma} \right] \quad (22a)$$

and

$$K_{db}^e(\omega_L) = 2i \left(\frac{\pi}{\gamma}\right)^{1/2} \sum_{a,c} \mu_{ab}\mu_{bc}\mu_{cd}\mu_{da} P(a) \times \frac{1}{\omega_L - \omega_{bc} + i\Gamma} \frac{\hat{\Gamma} + \gamma'}{(\omega_L - \omega_{da})^2 + \Gamma^2} \quad (22b)$$

Equations (19)–(22) are identical to the results of the optical Bloch equations.^{1,2}

$\chi^{(3)}$ for CARS in isolated molecules can be obtained from Eqs. (19)–(22) by setting $\hat{\Gamma} = 0$. An interesting cancellation takes place for the excited-state resonances in the absence of pure dephasing.¹⁰ The CARS excited-state resonance is contained in the following term in Eq. (19b):

$$\frac{\hat{\Gamma} + \gamma'}{\omega_L - \omega_{L'} - \omega_{db} + i\gamma} \quad (23)$$

When $\hat{\Gamma} = 0$ and $|a\rangle$ is the ground vibronic state, $\gamma' = \gamma_a = 0$ and the excited-state resonance vanishes, i.e.,

$$K_{db}^e(\omega_L) = 0. \quad (24)$$

The excited-state resonances are therefore dephasing induced.

C. Static (Inhomogeneous) Limit

The static limit is obtained when the fluctuations of the bath are extremely slow compared with their magnitude ($\kappa \ll 1$), and, in this case, the excited-state CARS resonances vanish owing to interference between the terms, just as with the isolated-molecule case. When $\Lambda \rightarrow 0$, all the n terms in Eq. (9a) contribute to the profile. In this limit, we have, by using a short-time approximation,

$$g(\tau) = \Delta^2 \tau^2 / 2. \quad (25)$$

After substitution of Eq. (25) into Eq. (9a) the infinite summation over n can be performed, giving

$$\chi_{ca}^{(3)} = \frac{1}{\sqrt{2\pi} \Delta} \int_{-\infty}^{\infty} d\omega \exp(-\omega^2/2\Delta^2) \sum_{b,d} \mu_{ab}\mu_{bc}\mu_{cd}\mu_{da} \times \frac{1}{\omega_L - \omega_{L'} - \omega_{ca} + i\gamma'} \frac{1}{2\omega_L - \omega_{L'} - \omega - \omega_{ba} + i\bar{\gamma}} \times \left[\frac{P(a)}{\omega_L - \omega - \omega_{da} + i\bar{\gamma}} + \frac{P(c)}{\omega_{dc} + \omega - \omega_{L'} + i\bar{\gamma}} \right]. \quad (26)$$

Table 1. Line-Broadening Parameters and Spectral Shifts for β -Carotene in Various Solvents^a

| Solvent | Temperature (K) | Pressure | ω_{eg} (cm ⁻¹) | Δ (cm ⁻¹) | Λ (cm ⁻¹) | Γ_0 (cm ⁻¹) | α (cm ⁻¹) |
|---------------------------------|-----------------|----------|-----------------------------------|------------------------------|-------------------------------|--------------------------------|------------------------------|
| Isopentane ^b | 118 | 1 bar | 20,180 | 413 (362) | 330 (108) | 700 (760) | 75 (0) |
| Isopentane ^c | 298 | 1 bar | 20,920 | 520 (581) | 520 (174) | 800 (1220) | 350 (0) |
| Carbon disulfide ^c | 298 | 1 bar | 19,300 | 374 (564) | 374 (56) | 850 (1280) | 375 (0) |
| Pentane-isopentane ^d | 298 | 70 kbar | 18,000 | 1250 (832) | 6250 (832) | 500 (1280) | 450 (0) |
| Pentane-isopentane ^e | 298 | 50 kbar | 18,150 | (619) | (62) | (1200) | (0) |
| Pentane-isopentane ^e | 298 | 20 kbar | 19,200 | (619) | (62) | (1200) | (0) |
| Pentane-isopentane ^e | 298 | 1 bar | 20,850 | (780) | (780) | (1200) | (0) |

^a Values in parentheses are best-fit parameters with no inhomogeneous broadening.

^b Experimental data from Ref. 14.

^c Experimental data from Ref. 18.

^d Experimental data from Ref. 16.

^e Experimental data from Ref. 15.

Table 2. Ground-State and Excited-State Frequencies and the Dimensionless Displacements Used in the Three-Mode Model Calculation of β -Carotene

| Mode | 1 | 2 | 3 |
|----------------------------------|------|------|------|
| ω_j'' (cm ⁻¹) | 1525 | 1155 | 1005 |
| ω_j' (cm ⁻¹) | 1580 | 1220 | 850 |
| D_j | 1.12 | 0.95 | 0.65 |

The CARS excitation amplitudes are given by

$$K_{ca}^g(\omega_L) = \frac{1}{\Delta(2\gamma)^{1/2}} \int_{-\infty}^{\infty} d\omega \exp(-\omega^2/2\Delta^2) \times \sum_{b,d} \mu_{ab}\mu_{bc}\mu_{cd}\mu_{da} \frac{1}{\omega_L - \omega - \omega_{bc} + i\gamma} \times \left[\frac{P(a)}{\omega_L - \omega - \omega_{da} + i\gamma} + \frac{P(c)}{\omega_{da} + \omega - \omega_L + i\gamma} \right] \quad (27a)$$

and

$$K_{db}^e(\omega_L) = 0. \quad (27b)$$

The excited-state CARS resonances vanish in this limit.

3. COMPARISON OF SPONTANEOUS AND COHERENT RAMAN EXCITATION PROFILES OF β -CAROTENE

Trans- β -carotene (Fig. 4) is one of the first polyatomic molecules for which detailed spontaneous Raman excitation profiles were measured.¹¹ Its strong absorption in the visible region and low fluorescence yield make it an ideal system for Raman measurements. β -carotene has a simple well-resolved Raman progression consisting of only three strong optically active vibrational modes. This makes it most suitable for theoretical analysis. β -carotene is an important biological molecule present in great quantities in many plants and is believed to play a critical role in photosynthesis. In the human body, it is a vitamin A precursor. β -carotene also possesses several properties of chemical interest. It is a substituted polyene, a class of molecules that has been the subject of considerable interest,¹² and it is also a model system for the organic conductor polyacetylene. Spontaneous Raman excitation profiles of β -carotene in alkanes, benzene, toluene, acetone, and ethyl alcohol have been investigated by a number of workers.¹¹⁻²⁰ In all these works a three-mode model was adopted that included all the strongly optically active modes. In this paper we adopt the same model. Many of these analyses did not consider the dynamics of solvation and assumed a three-mode model with only lifetime broadening. Siebrand and co-workers have assumed, in addition to lifetime broadening, a Gaussian inhomogeneous broadening mechanism.¹³ Ho and co-workers postulated a bath of identical harmonic low-frequency modes as a broadening mechanism,¹⁴⁻¹⁶ and Lee *et al.* used a transform technique to relate the absorption line shape to the Raman excitation profiles.¹⁷ β -carotene is also one of the few molecules for which coherent Raman excitation profiles are available. Carreira *et al.* measured the

CARS profiles of two fundamentals of β -carotene in benzene and analyzed their results assuming a Lorentzian broadening.²¹

β -carotene has three optically active vibrational modes, with ground-state frequencies $\omega_1'' = 1525$ cm⁻¹, $\omega_2'' = 1155$ cm⁻¹, and $\omega_3'' = 1005$ cm⁻¹. The first two modes are the C—C and the C—C stretching modes, respectively, and the third mode is a CH₃ in-plane rocking mode.²⁰ In our model calculations on β -carotene we assumed a three-mode displaced harmonic oscillator model, i.e.,

$$H_g = \frac{1}{2} \sum_{j=1}^3 \omega_j'' (p_j'' + q_j'' - 1), \quad (28a)$$

$$H_e = \frac{1}{2} \sum_{j=1}^3 \omega_j' (p_j' + q_j' - 1). \quad (28b)$$

The dimensionless momentum and coordinate corresponding to the j 'th normal mode are denoted by p_j'' and q_j'' , respectively, in the ground state and by p_j' and q_j' in the excited state. The normal-mode coordinates are related by the transformation

$$q_j' = (\omega_j'/\omega_j'')^{1/2} q_j'' + D_j, \quad (29)$$

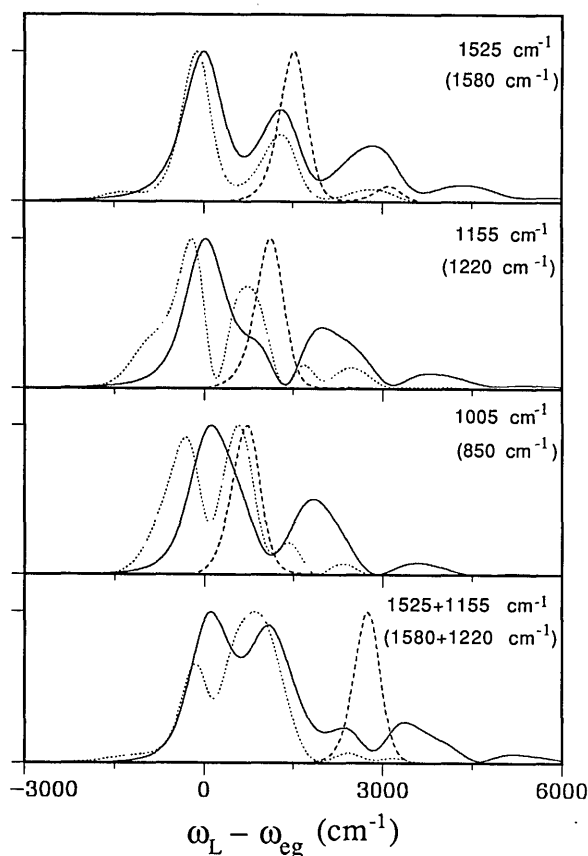


Fig. 6. Ground-state CARS (dotted lines) and excited-state CARS (dashed lines) resonance excitation profiles $Q^i(\omega_L)$ [Eq. (30)] of β -carotene in isopentane at 118 K. For comparison, the spontaneous Raman profiles of Figs. 4 and 5 (solid lines) are shown. The ground-state Raman frequencies and the excited-state Raman frequencies (in parentheses) are given. All curves were normalized to the same maximum peak value. The solvent parameters are (in cm⁻¹): $\omega_{eg} = 20\,180$, $\alpha = 75$, $\Gamma_0 = 700$, $\Delta = 413$, $\Lambda = 330$.

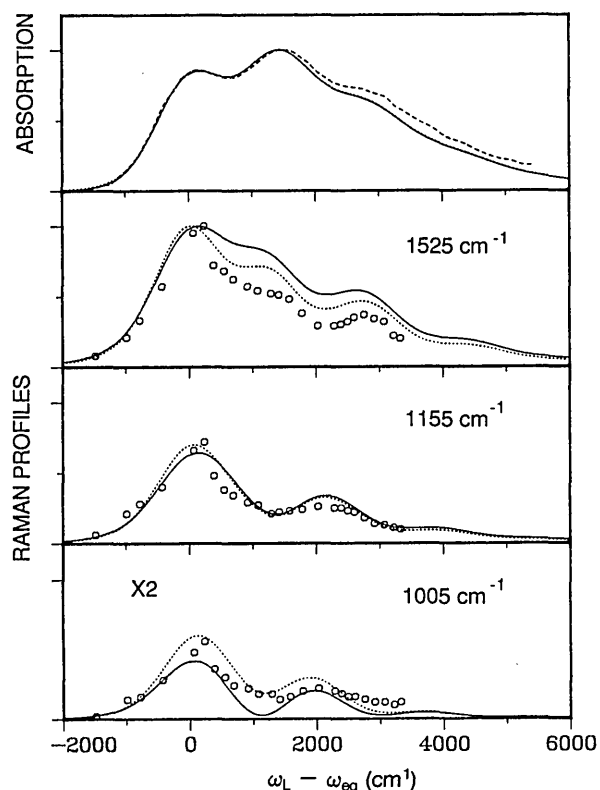


Fig. 7. Absorption $\sigma(\omega_L)$ (upper panel) and relative resonance Raman profiles $Q_{ca}(\omega_L)$ of the indicated transitions (three lower panels) of β -carotene in isotentane at 298 K. The dashed curve in the upper panel and the circles in the three lower panels are the experimental data of Ref. 14. $\omega_{eg} = 20\,920\text{ cm}^{-1}$, and the solvent parameters are (in cm^{-1}) solid lines: $\alpha = 0$, $\Gamma_0 = 1220$, $\Delta = 581$, $\Lambda = 174$; dotted lines: $\alpha = 350$, $\Gamma_0 = 800$, $\Delta = 520$, $\Lambda = 520$.

where D_j is the dimensionless displacement between the equilibrium positions of the potential surfaces of mode j . In solution, the time scale of the fluctuations of the energy gap due to solvent-solute collisions is typically fast compared with molecule lifetimes (the rapid fluctuation limit), but, in addition, there may also be an inhomogeneous variation in the energy gap with energy distribution $S(\omega)$ because of slow molecular processes (e.g., conformational broadening). We further note that in harmonic molecules the levels are equally spaced, and there may be several pairs of a , c (or b , d) levels with the same Raman frequency. In this case, the Raman amplitudes have to be summed over all the possible transitions with the same Raman frequency [Eq. (14e)]. The CARS excitation profiles are thus given by

$$Q^i(\omega_L) = \left[\int_{-\infty}^{\infty} d\omega S(\omega) \left[\sum'_{a,c} K_{ca}^g(\omega_L - \omega) + \sum'_{b,d} K_{bd}^e(\omega_L - \omega) \right] \right]^2, \quad (30)$$

where the Raman amplitudes K_{ac}^g and K_{bd}^e are given by Eqs. (17). The corresponding spontaneous Raman excitation profiles $Q_{ca}(\omega)$ and the absorption line shape $\sigma(\omega)$ for this model are given by^{7,8}

$$Q_{ca}(\omega_L) = 2\pi P(a) \int_{-\infty}^{\infty} d\omega S(\omega) |K_{ca}(\omega_L - \omega)|^2 \quad (31)$$

and

$$\sigma(\omega_L) = -2\omega_L \text{Im} \int_{-\infty}^{\infty} d\omega S(\omega) \sum_a P(a) K_{aa}(\omega_L - \omega), \quad (32)$$

where

$$K_{ca}(\omega_L) = \sum_b \mu_{cb} \mu_{ba} J_0(\omega_L - \omega_{ba} + i\bar{\gamma}). \quad (33)$$

Note that the averaging over the static distribution $S(\omega)$ is at the amplitude level in the case of CARS and at the intensity (amplitude square) level for spontaneous Raman spectroscopy. In general, $S(\omega)$ may take any form, but it is often taken to be Gaussian, i.e.,

$$S(\omega) = (2\pi\alpha)^{-1/2} \exp(-\omega^2/2\alpha^2). \quad (34)$$

This may be rationalized by using the central-limit theorem since the broadening usually results from many small contributions. It is possible to recast the excitation-profile amplitudes Eqs. (17) and (33) in an eigenstate-free form^{4,5,22}:

$$K_{ca}^g(\omega_L) = (\pi/\gamma')^{1/2} P(a) G_{ac}(\epsilon_c + \omega_L) [G_{ac}(\epsilon_a + \omega_L) - \exp(-\omega_{ca}/kT) G_{ac}^*(\epsilon_a + \omega_L)], \quad (35a)$$

$$K_{db}^e(\omega_L) = 2i(\pi/\gamma')^{1/2} \bar{G}_{db}^*(\epsilon_b - \omega_L) \text{Im} \bar{G}_{db}(\epsilon_d - \omega_L), \quad (35b)$$

$$K_{ca}(\omega_L) = G_{ca}(\epsilon_a + \omega_L), \quad (35c)$$

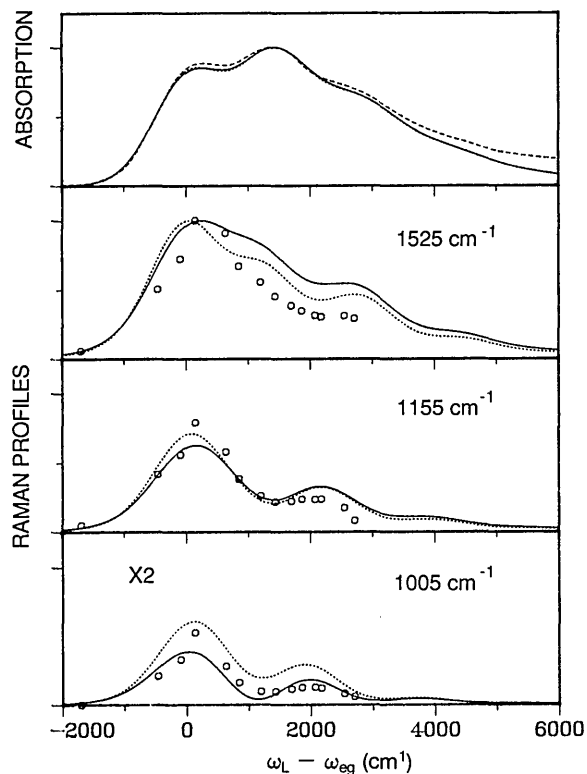


Fig. 8. Absorption $\sigma(\omega_L)$ (upper panel) and relative resonance Raman profiles $Q_{ca}(\omega_L)$ of the indicated transitions (three lower panels) of β -carotene in CS_2 at 298 K. The dashed curve in the upper panel and the circles in the three lower panels are the experimental data in Ref. 18. We estimated the relative intensities from the 514.5-nm excitation dispersed emission given in Fig. 2 of Ref. 18. $\omega_{eg} = 19\,300\text{ cm}^{-1}$, and the solvent parameters are (in cm^{-1}) solid lines: $\alpha = 0$, $\Gamma_0 = 1280$, $\Delta = 564$, $\Lambda = 56$; dotted lines: $\alpha = 375$, $\Gamma_0 = 650$, $\Delta = 374$, and $\Lambda = 374$.

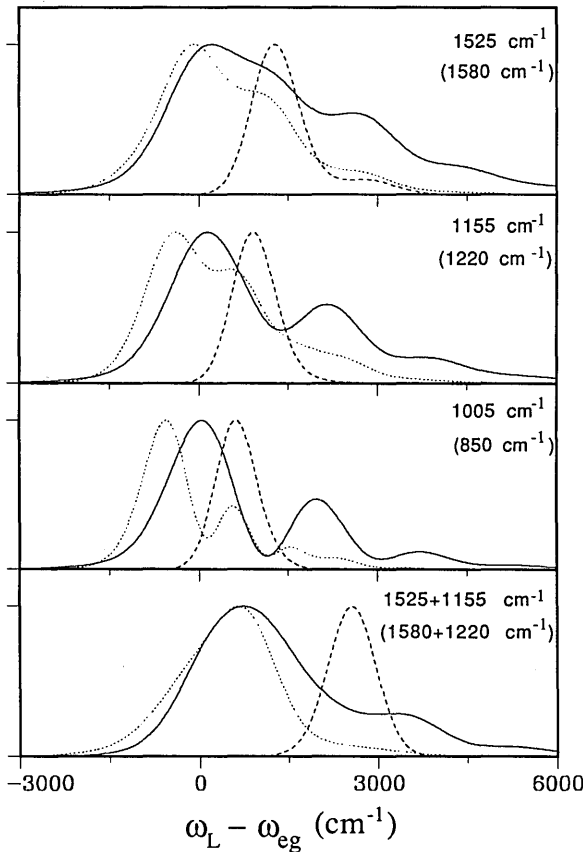


Fig. 9. Ground-state CARS (dotted lines) and excited-state CARS (dashed lines) resonance excitation profiles $Q^i(\omega_L)$ of β -carotene in CS_2 at 298 K assuming no inhomogeneous broadening. For comparison, the spontaneous Raman profiles $Q_{ca}(\omega_L)$ of Fig. 8 (solid lines) are shown. All curves have been normalized to the same maximum peak value. The ground-state Raman frequencies and the excited-state Raman frequencies (in parentheses) are given. Solvent parameters used in the calculation are (in cm^{-1}) $\omega_{eg} = 19\,300$, $\alpha = 0$, $\Gamma_0 = 1280$, $\Delta = 564$, $\Lambda = 56$.

where

$$G_{ca}(\omega) = -i \int_0^\infty d\tau \exp[i\omega\tau - g(\tau)] \langle c | \exp(-iH_e\tau) | a \rangle, \quad (36a)$$

$$\tilde{G}_{db}(\omega) = -i \int_0^\infty d\tau \exp[i\omega\tau - g(\tau)] \langle d | \exp(-iH_g\tau) | b \rangle, \quad (36b)$$

$$\bar{G}_{db}(\omega) = -i \int_0^\infty d\tau \exp[i\omega\tau - g(\tau)] \langle d | \exp[-iH_g(i\tau + 1/kT)] | b \rangle. \quad (36c)$$

Simple expressions for Eqs. (36) for general harmonic molecules have been derived.^{5,7,8,22} They eliminate the summations over intermediate states, which is the limiting step in the calculation of nonlinear susceptibilities in large polyatomic molecules.

We applied this model to some experimental Raman data of β -carotene in various solvents. Our procedure was first to fit the well-resolved low-temperature (118-K) absorption line shape and the spontaneous Raman profiles of β -carotene in isopentane that were obtained by Ho *et al.*¹⁴ In the calculations of Eqs. (30)–(36) we utilize a standard fast-Fourier-transform routine on 8192 time points with a step size $\Delta t = 6.4 \times 10^{-15}$ sec. The structural parameters (dis-

placements, excited-state frequencies) thus obtained were then used to fit other experimental data by changing only the solvent-broadening parameters (Δ , Λ , α) and the 0–0 transition frequency (ω_{eg}). The results of our 118-K isopentane calculations (the absorption and spontaneous Raman profile of the three fundamentals and four combinations) are displayed in Figs. 4 and 5. In each figure we show the best fit obtained without inhomogeneous broadening ($\alpha = 0$) and with inhomogeneous broadening ($\alpha = 75 \text{ cm}^{-1}$). The results show that inhomogeneous broadening is relatively unimportant at this temperature. The solvation parameters are given in Table 1. The structural parameters used in the fit are given in Table 2 and were used in all the following calculations. The frequencies of the three optically active modes all changed appreciably (4–15%) on excitation. The excited-state CARS resonances should therefore be distinguishable from the ground-state resonances. Figure 6 shows the predicted CARS excitation profiles for the indicated Raman transitions calculated by using the best-fit parameters ($\alpha = 75 \text{ cm}^{-1}$) of Figs. 4 and 5. The calculations performed by using no inhomogeneous broadening ($\alpha = 0$) are not significantly different in this case and are not shown. The CARS excitation profiles of β -carotene in benzene measured by Carreira *et al.*²¹ show similar structure. The limit-

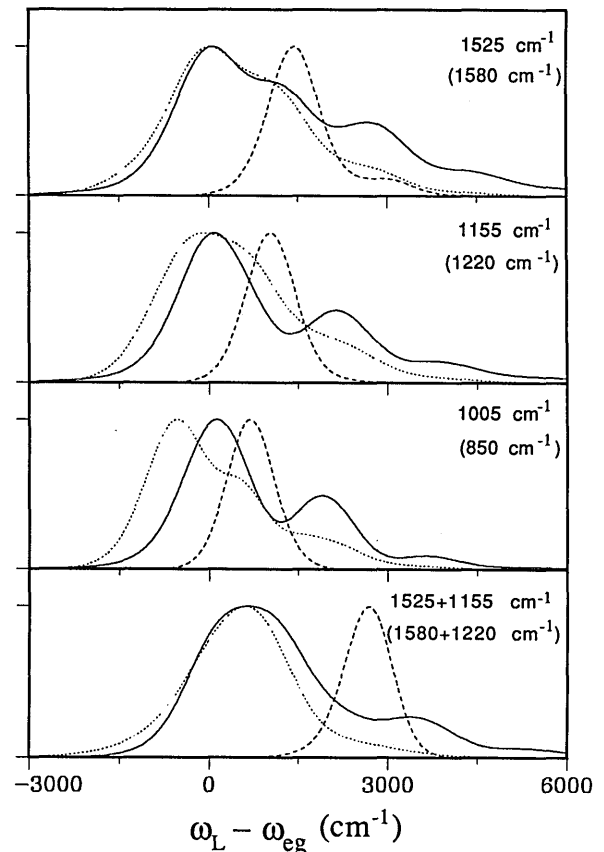


Fig. 10. Ground-state CARS (dotted lines) and excited-state CARS (dashed lines) resonance excitation profiles $Q^i(\omega_L)$ of β -carotene in CS_2 at 298 K assuming both homogeneous and inhomogeneous broadening. For comparison, the spontaneous Raman profiles $Q_{ca}(\omega_L)$ of Fig. 8 (solid lines) are shown. All curves have been normalized to the same maximum peak value. The ground-state Raman frequencies and the excited-state Raman frequencies (in parentheses) are given. Solvent parameters used in the calculation are (in cm^{-1}): $\omega_{eg} = 19\,300$, $\alpha = 375$, $\Gamma_0 = 850$, $\Delta = 374$, and $\Lambda = 374$.

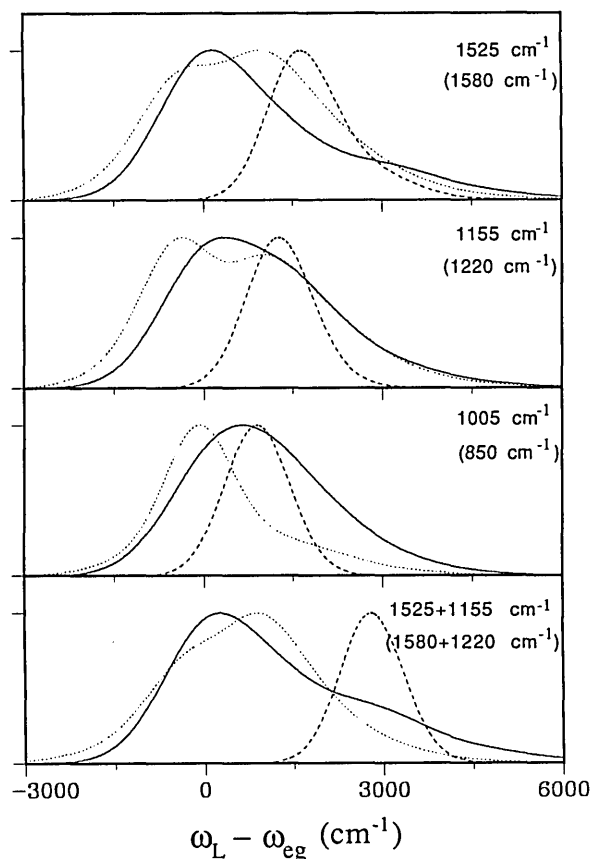


Fig. 11. Ground-state CARS (dotted lines) and excited-state CARS (dashed lines) excitation profiles $Q^i(\omega_L)$ and spontaneous Raman excitation profiles $Q_{ca}(\omega_L)$ (solid lines) of β -carotene in CS_2 at 298 K assuming the broadening is almost entirely inhomogeneous. All curves have been normalized to the same maximum peak value. The ground-state Raman frequencies and the excited-state Raman frequencies (in parentheses) are given. Solvent parameters used in the calculation are (in cm^{-1}): $\omega_{eg} = 19\,300$, $\alpha = 750$, $\Gamma_0 = 100$, $\Delta = 83$, $\Lambda = 83$.

ed experimental information does not permit a more quantitative analysis in this case. For comparison, we also show the spontaneous Raman profiles. Note that in each panel the main peak of the excited-state CARS is shifted to the blue with respect to the 0-0 transition frequency by an amount approximately equal to the Raman frequency. This can be understood as follows: according to Eq. (17b), a peak occurs when ω_L is resonant with the da transition, where level a is the ground vibronic state. Since the excited-state vibronic levels b and d are specified by the condition $\omega_{db} = \omega_L - \omega_L'$, level d must be an excited vibronic state, and the resonant peak occurs at $\omega_L = \omega_{da}$ and not at $\omega_L = \omega_{eg}$. Figures 7 and 8 show the absorption line shape and the spontaneous Raman profiles of the three fundamentals of β -carotene at 298 K in isopentane and in CS_2 , respectively. In each case we have calculated the best fit with and without inhomogeneous broadening. The calculated Raman profiles with inhomogeneous broadening are considerably better. Compared with the 118-K calculation, the room-temperature fits indicate that inhomogeneous broadening plays an increasingly important role at higher temperatures. Figures 9 and 10 show the predicted CARS excitation profiles of β -carotene in CS_2 by using the same parameters of Fig. 8. In

comparing the two figures, it is apparent that there is less vibrational structure in the line shapes when inhomogeneous broadening is present (Fig. 10). We have also calculated (Fig. 11) the CARS profiles assuming that almost all the broadening is inhomogeneous ($\alpha = 750 \text{ cm}^{-1}$). Figures 12 and 13 show some fitted high-pressure data of β -carotene in a 1:1 mixture of pentane-isopentane. Figure 12 shows the calculated and the experimental absorption line shapes and Raman profiles at 70 kbars. The relative contribution of inhomogeneous broadening to the total broadening is also significant in this case. Figure 13 shows the absorption line shapes at four different pressures. The fits are good, which suggests that the structural parameters are insensitive to the ambient pressure. No inhomogeneous broadening was used in the calculation in Fig. 13 since absorption line shapes are sensitive only to the total broadening present and not to its nature. Without supporting Raman data, the solvation parameters (Δ , Λ) obtained for the pentane-isopentane mixtures should be treated with caution.

Our calculations of the 118- and 298-K isopentane spectra show that both the magnitude Δ and the inverse time scale Λ of the random force exerted by the bath on the three-mode system increase significantly with temperature. This may be understood in terms of an increase in the rate and kinetic energy of solvent collisions. It should be emphasized that

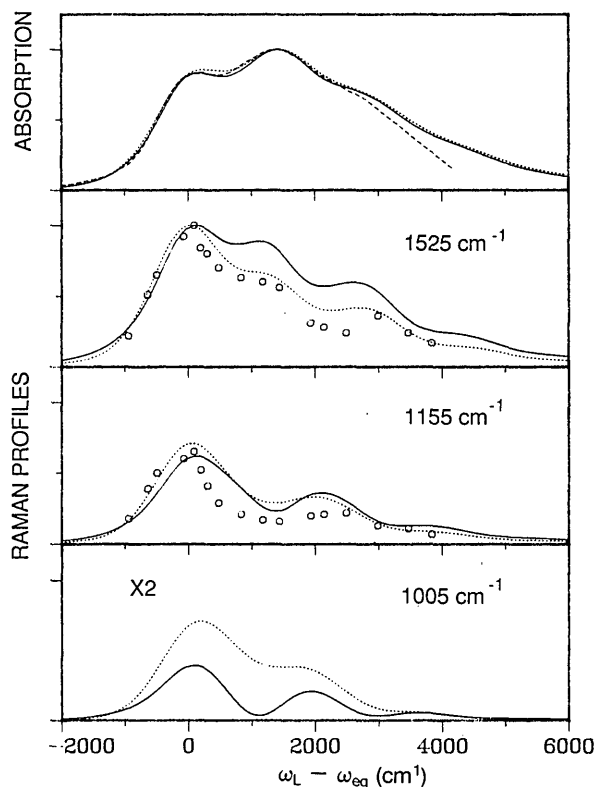


Fig. 12. High-pressure (70-kbar) absorption $\sigma(\omega_L)$ (upper panel) and relative resonance Raman profiles $Q_{ca}(\omega_L)$ of the indicated transitions (three lower panels) of β -carotene in a 1:1 pentane-isopentane mixture at 298 K. The dashed curve in the upper panel and the circles (two middle panels) are the experimental data of Ref. 16, where $\omega_{eg} = 18\,000 \text{ cm}^{-1}$ and the solvent parameters are (in cm^{-1}) solid lines: $\alpha = 0$, $\Gamma_0 = 1280$, $\Delta = 832$, $\Lambda = 832$; dotted lines: $\alpha = 450$, $\Gamma_0 = 500$, $\Delta = 1250$, $\Lambda = 6250$.

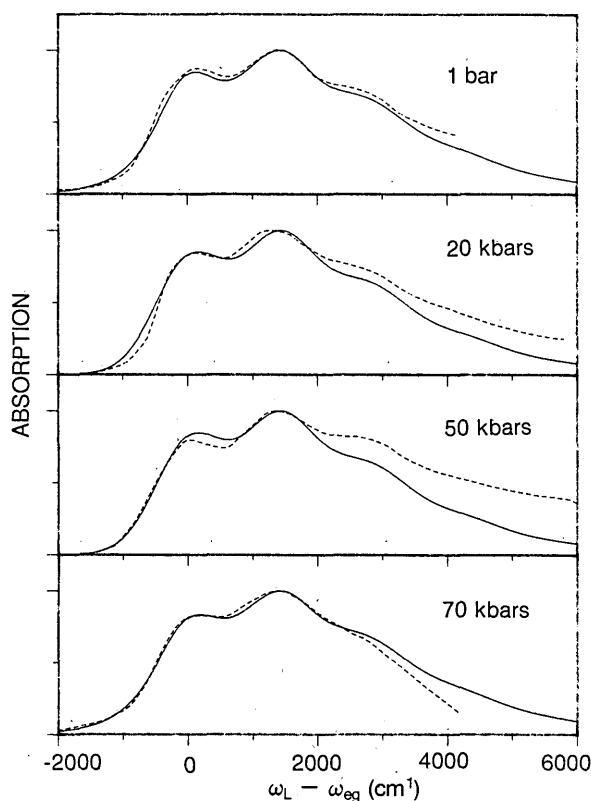


Fig. 13. Absorption line shapes $\sigma(\omega_L)$ of β -carotene in a 1:1 pentane-isopentane mixture at the four pressures indicated. The experimental curves (dashed lines) are from Ref. 15. The solid lines are the theoretical calculations using the structural parameters of Table 2, and the solvent parameters are (in cm^{-1}) 1 bar: $\alpha = 0$, $\Gamma_0 = 1200$, $\Delta = 780$, $\Lambda = 780$, $\omega_{eg} = 20\,850$; 20 kbars: $\alpha = 0$, $\Gamma_0 = 1200$, $\Delta = 619$, $\Lambda = 62$, $\omega_{eg} = 19\,200$; 50 kbars: $\alpha = 0$, $\Gamma_0 = 1200$, $\Delta = 619$, $\Lambda = 62$, $\omega_{eg} = 18\,150$; 70 kbars: $\alpha = 0$, $\Gamma_0 = 1280$, $\Delta = 832$, $\Lambda = 832$, $\omega_{eg} = 18\,000$.

the bath in our model includes low-frequency modes as well as the solvent. Undoubtedly some low-frequency modes contribute to the random force experienced by the system,²³ but extremely low-frequency modes with periods large compared with the lifetime of the excited state will contribute to the inhomogeneous broadening instead. Thermal excitation of the latter modes may explain the increase in the inhomogeneous broadening α from 75 cm^{-1} at 118 K to 350 cm^{-1} at 298 K. Schomacker and co-workers²⁴ have examined the role of low-frequency modes in the spectra of cytochrome *c* and have found that their effects on the line shapes are negligible. Their model assumed a bath of identical low-frequency harmonic modes in the short-time approximation and temperature-independent inhomogeneous broadening. In this paper the treatment of the bath (low-frequency modes and the solvent) is more general, and we cannot rule out a significant contribution from the low-frequency modes to the line shapes. The displacements D_j (Table 2) are in good agreement with previous results.¹¹⁻²¹ We found that the excited-state frequency was larger than the ground-state frequency for modes one and two ($\omega_1' = 1525$, $\omega_1'' = 1580$, $\omega_2' = 1155$, $\omega_2'' = 1220\text{ cm}^{-1}$) and smaller for mode three ($\omega_3' = 1005\text{ cm}^{-1}$, $\omega_3'' = 850\text{ cm}^{-1}$), whereas in previous analyses the excited-state and ground-state frequencies were assumed to be identical. The best-fit parameters for the various sol-

vents are summarized in Table 1. The agreement of the absorption line shape and Raman-excitation profiles is better, and our theoretical treatment is more complete compared with earlier works. Since the effect of pure dephasing is properly incorporated, we did not need to assume ultra-short lifetimes.^{11,18-21} In contrast to previous treatments, our model permits the calculation of the fluorescence in spontaneous light scattering and the calculation of the background signal in coherent Raman spectroscopy. We have used a similar model to analyze the fluorescence line shapes of tetrademethyl- β -carotene, resulting in a detailed picture of its excited-state dynamics.⁸

4. CONCLUDING REMARKS

We have analyzed in detail a stochastic theory for coherent Raman line shapes that is valid for an arbitrary time scale of the bath. This theory interpolates between the homogeneous limit, in which the Bloch equations are valid, and the static limit of inhomogeneous line broadening. Application was made to the β -carotene molecule in several solvents, and the spontaneous Raman and CARS excitation profiles were compared. The calculated spontaneous Raman profiles were found to be in good agreement with experiment, and the CARS profiles were predicted. Our calculations indicate that at room temperature, in addition to homogeneous line broadening, there is also significant inhomogeneous broadening. Solvent time scales and interaction strengths were extracted in all cases and are given in Table 1.

ACKNOWLEDGMENT

S. Mukamel is a Camille and Henry Dreyfus Teacher-Scholar.

J. Sue is also with the Department of Physics and Astronomy, University of Rochester.

REFERENCES

1. M. D. Levenson, *Introduction to Nonlinear Laser Spectroscopy* (Academic, New York, 1987).
2. Y. R. Shen, *The Principles of Nonlinear Optics* (Wiley, New York, 1984).
3. S. Mukamel and R. F. Loring, *J. Opt. Soc. Am. B* **3**, 595 (1986); R. F. Loring and S. Mukamel, *J. Chem. Phys.* **83**, 2116 (1985); S. Mukamel, *Phys. Rev. A* **28**, 3480 (1983).
4. Z. Deng and S. Mukamel, *J. Chem. Phys.* **85**, 1738 (1986).
5. S. Mukamel, *J. Chem. Phys.* **82**, 5398 (1985); *Adv. Chem. Phys.* **70**, 155 (1988).
6. J. Tang and A. C. Albrecht, in *Raman Spectroscopy*, H. A. Szymanski, ed. (Plenum, New York, 1970), Vol. 2, p. 33; P. M. Champion and A. C. Albrecht, *Annu. Rev. Phys. Chem.* **33**, 353 (1982).
7. J. Sue, Y. J. Yan, and S. Mukamel, *J. Chem. Phys.* **85**, 462 (1986).
8. J. Sue and S. Mukamel, *J. Chem. Phys.* **88**, 651 (1986).
9. R. Kubo, *Adv. Chem. Phys.* **15**, 101 (1969); A. Kotani and Y. Toyozawa, *J. Phys. Soc. Jpn.* **41**, 1699 (1976).
10. N. Bloembergen, H. Lotem, and R. T. Lynch, *Indian J. Pure Appl. Phys.* **16**, 151 (1978); J. R. Andrews and R. M. Hochstrasser, *Chem. Phys. Lett.* **82**, 381 (1981); J. R. Andrews, R. M. Hochstrasser, and H. P. Trommsdorff, *Chem. Phys.* **62**, 87 (1981).
11. S. Saito, M. Tasumi, and C. H. Eugster, *J. Raman Spectrosc.* **14**, 299 (1983); F. Inagaki, M. Tasumi, and T. Miyazawa, *J. Mol. Spectrosc.* **50**, 286 (1974).

12. B. S. Hudson, B. E. Kohler, and K. Schulten, in *Excited States*, E. C. Lim, ed. (Academic, New York, 1984), Vol. 6.
13. W. Siebrand and M. Z. Zgierski, *J. Chem. Phys.* **71**, 3561 (1979); M. Samoc, W. Siebrand, D. F. Williams, E. G. Woolgar, and M. Z. Zgierski, *J. Raman Spectrosc.* **11**, 369 (1981); A. P. Penner and W. Siebrand, *Chem. Phys. Lett.* **39**, 11 (1976).
14. Z. Z. Ho, T. A. Moore, S. H. Lin, and R. C. Hanson, *J. Chem. Phys.* **74**, 873 (1981).
15. Z. Z. Ho, R. C. Hanson, and S. H. Lin, *J. Chem. Phys.* **77**, 3414 (1982).
16. Z. Z. Ho, R. C. Hanson, and S. H. Lin, *J. Phys. Chem.* **89**, 1014 (1985).
17. S. A. Lee, C. K. Chan, J. B. Page, and C. T. Walker, *J. Chem. Phys.* **84**, 2497 (1986).
18. S. Sufra, G. Dellepiane, G. Masetti, and G. Zerbi, *J. Raman Spectrosc.* **69**, 142 (1972).
19. L. C. Hoskins, *J. Chem. Phys.* **72**, 4487 (1980).
20. S. Saito and M. Tasumi, *J. Raman Spectrosc.* **14**, 236, 310 (1983).
21. L. A. Carriera, T. C. Maguire, and T. Malloy, Jr., *J. Chem. Phys.* **66**, 2621 (1977).
22. Y. J. Yan and S. Mukamel, *J. Chem. Phys.* **85**, 5908 (1986).
23. K. Shan, Y. J. Yan, and S. Mukamel, *J. Chem. Phys.* **87**, 2021 (1987).
24. K. T. Schomacker and P. M. Champion, *J. Chem. Phys.* **84**, 5314 (1986); K. T. Schomacker, V. Srajer, and P. M. Champion, *J. Chem. Phys.* **86**, 1796 (1987); L. Reinisch, K. T. Schomacker, and P. M. Champion, *J. Chem. Phys.* **87**, 150 (1987).